D 5 Quasielastic Scattering

Joachim Wuttke
Jülich Centre for Neutron Science
Forschungszentrum Jülich GmbH

Contents

Lecture Notes of the 50^{th} IFF Spring School "Scattering! Soft, Functional and Quantum Materials".

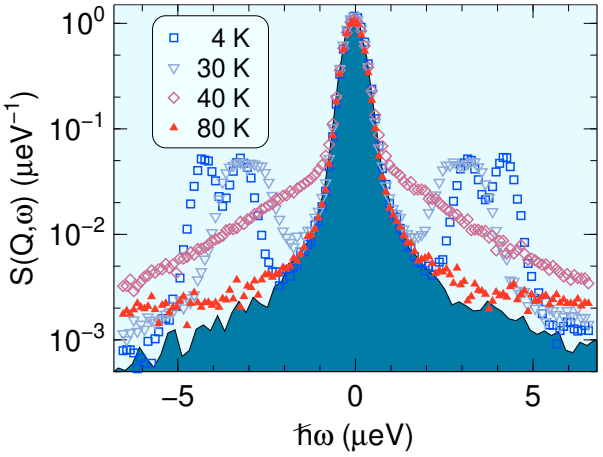

Fig. 1: Neutron backscattering spectra of an organic ionic crystal (2:1 picric acid and tetramethylpyrazine) [1], measured on SPHERES. The inelastic features are due to methyl group rotation. With increasing temperature, they soften and broaden and finally merge into a quasielastic central peak, due to the crossover from tunneling to thermally activated jumps. The dark area marks the resolution function, measured using an elastic standard scatterer.

1 Introduction

Quasielastic neutron scattering (QENS) is inelastic scattering, measured with fine energy resolution, and used for the study of motions that are much slower than typical vibration modes. In this chapter, we will discuss different kinds of *slow motion*. But first, we should explicate the term *quasielastic*.

The term *quasielastic scattering* comes from nuclear physics; it designates the limiting case of inelastic scattering, close to elastic scattering, where the energy transfer is much smaller than the incident energy of the scattered particles.[1]

The term *quasielastic peak* (or *line*) designates a spectral distribution that is centered around $\hbar\omega \simeq 0$. It can be seen as a broadened elastic peak, in the same way as a Gaussian or a Lorentzian can be seen as a broadened delta function.

These three criteria (slow motion, small energy transfer, broadened elastic peak) are fuzzy, and only weakly correlated. In practice, whatever can be subsumed under one of them may be designated as QENS. Any stricter terminology would collide with the manyfold borderline and crossover cases of which examples are given in Figs. 1 and 2. In both examples, a meaningful analysis of the quasielastic high-temperature peaks is only possible if their relation to some inelastic low-temperature modes is taken into consideration.

Fig. 1 shows backscattering spectra of an organic crystals. With an energy window $|\hbar\omega| < 7$ μeV and a fixed final neutron energy $E_\mathrm{f} = 2.08$ meV, this is clearly quasielastic scattering in the sense $|\hbar\omega| \ll E_\mathrm{f}$. All scattering intensity beyond the resolution-broadened elastic line is due to methyl group rotation. At low temperature, there are two pairs of inelastic lines. With increasing temperature, they soften, broaden, and merge into one quasielastic peak, revealing the crossover from quantum tunneling to thermally activated jumps (Sects. 4.3–4.4).

Fig. 2 shows time-of-flight spectra of an ionic solution in the glassy and liquid state. The energy

[1] In light scattering, the terminology is particularly confused. The light scattering analogue of quasielastic neutron scattering employs a grating spectrometer or a Fabry-Perot interferometer to analyse the energy of scattered photons; these techniques are commonly called *high-resolution inelastic light scattering* or *Rayleigh-Brillouin scattering*. In contrast, in *quasielastic light scattering*, also called *dynamic light scattering* or (much more to the point) *photon correlation spectroscopy*, scattered photons are counted regardless of their energy; photon counts are then correlated by some real-time circuitry.

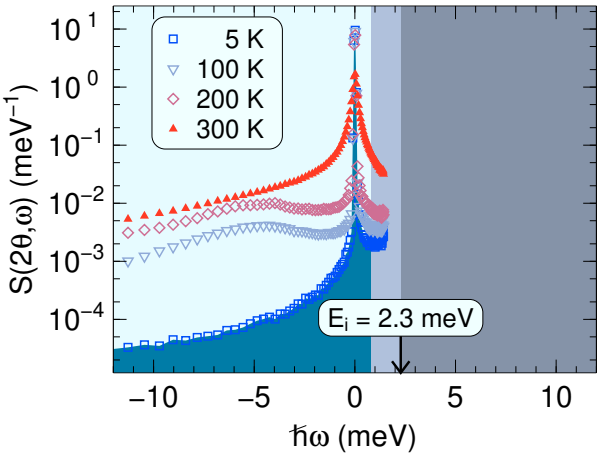

Fig. 2: Neutron time-of-flight spectra of a LiCl:H_2O solution [2], measured on TOFTOF. They dark gray area on the right is kinematically inaccessible. In the light gray stripe with $\hbar\omega \lesssim E_\mathrm{i}$, data analysis is not possible because scattered neutrons are so slow that they are overtaken by the next pulse (*frame overlap*). The broad maximum around 5 meV is typical for glasses (*boson peak*); in the liquid state (at 300 K), there is a broad quasielastic peak.

window extends to a multiple of the incident neutron energy $E_\mathrm{i} = 2.3$ meV. This is clearly not quasielastic in the sense $|\hbar\omega| \ll E_\mathrm{f}$. However, at 300 K there is a quasielastic peak: centered around $\hbar\omega \simeq 0$, and substantially broader than the resolution (measured using the same sample at 5 K). It is due to structural relaxation (Sect. 4.6), and with decreasing temperature becomes so narrow that it is no longer resolved by TOFTOF, leaving only an inelastic phonon spectrum.

Also in the following, all examples will come from time-of-flight or backscattering spectrometers. The spin-echo method, which is special in several respects (implicit Fourier transform, preference for coherent scattering and small Q), shall be left to another chapter (D6).

Much, but not all of the following, is covered in depth in the monographies [3–5]. I have not yet seen the forthcoming book [6].

2 Measuring the double differential cross section

When textbooks say that inelastic neutron scattering measures the double differential cross section $\partial^2\sigma/\partial\Omega/\partial\omega$, then this is a typical pedagogical simplification. Experimentalists need to understand the dependence of recorded neutron counts on the sample properties in more detail so that they can assess possible distortions and apply appropriate corrections. Here we briefly present the two biggest concerns, multiple scattering and instrumental resolution.

2.1 Attenuation and multiple scattering

Scattering from a small sample is described by the double-differential cross section, which gives the number of neutrons per time and per incident flux that are scattered into a solid angle $\mathrm{d}\Omega$ and a frequency interval $\mathrm{d}\omega$. In real samples, however, some neutrons are scattered more than once. In single crystals, coherent multiple scattering of waves leads to a variety of effects (D3) that are studied by dynamical diffraction theory. In powders and in disordered systems, and also in inelastic scattering from single crystals, these interference effects play no role because the coherence length of scattered radiation is much smaller than the mean free path. Therefore we shall discuss multiple scattering in terms not of wave functions, but of particle currents.

This is the domain of *transport theory*. The neutron distribution in phase space, $f(\mathbf{r}, \mathbf{k}, t)$, obeys

a Boltzmann equation. We request a solution in form of a multiple-scattering expansion $f = \sum_{j=0} f_j$, where f_j is the distribution of neutrons that have been scattered j times. The stationary Boltzmann equation, brought into recursive form, is solved by [7, 8]

$$\begin{aligned} f_0(\mathbf{r},\mathbf{k}) &= f_0(\mathbf{r} - L_{\mathbf{r},\hat{\mathbf{k}}}\hat{\mathbf{k}},\mathbf{k})\,\mathrm{e}^{-\Sigma(k)L_{\mathbf{r},\hat{\mathbf{k}}}}, \\ f_j(\mathbf{r},\mathbf{k}) &= \int \mathrm{d}^3k'\,\Gamma(\mathbf{k}',\mathbf{k}) \int_0^{L_{\mathbf{r},\hat{\mathbf{k}}}} \mathrm{d}\xi\,\mathrm{e}^{-\Sigma(k)\xi}\, f_{j-1}(\mathbf{r}-\xi\hat{\mathbf{k}},\mathbf{k}'), \end{aligned} \tag{1}$$

where $j \geq 1$, $\mathbf{r}$ is inside the sample, $L_{\mathbf{r},\hat{\mathbf{k}}}$ is the distance from $\mathbf{r}$ in direction $\hat{\mathbf{k}}$ to the sample surface, $\Sigma = \Sigma_\mathrm{a} + \Sigma_\mathrm{s}$ is the probability per unit length for loss by absorption or scattering, and $\Gamma(\mathbf{k}',\mathbf{k})\mathrm{d}^3k$ is the probability per unit length for scattering from wavevector $\mathbf{k}'$ towards an element d^3k around $\mathbf{k}$, given by the transference function

$$\Gamma(\mathbf{k}',\mathbf{k}) = \frac{\hbar}{m}\frac{k'}{k^2}\frac{1}{V}\frac{\partial^2\sigma}{\partial\Omega\partial\omega}, \tag{2}$$

where V is the volume associated with the double differential cross section.

The single-scattering intensity, given by f_1, is proportional to $\partial^2\sigma/\partial\Omega\partial\omega$. It differs from the thin-sample limit by exponential attenuation factors. For a simple sample geometry and a homogenous incident beam, the ξ integral in (1) can be carried out analytically to yield a single attenuation factor $\mathcal{A}(\Sigma(k_\mathrm{in}),\Sigma(k_\mathrm{out}))$. The multiple-scattering terms for $j \geq 2$ contain self-convolutions of the transference function and increasingly complicated attenuation factors.

In inelastic scattering, as long as one is only interested in the central frequency, width, and approximate intensity of excitation lines, attenuation and multiple scattering are of little concern. Multiple scattering by dispersionless excitations would generate peaks at overtone and combination frequencies, but in practice the excitation frequency *does* depend on Q. Since multiple scattering involves a convolution in Q, it averages over peaks at different frequencies, and results in a smooth background against which the single-scattering peaks stand out. In contrast, when it comes to the width, intensity, and lineshape of quasielastic peaks, then multiple scattering can cause severe distortions and spurious results [9], and therefore ought to be examined more often than in current QENS practice.

Inverting the dependence of f on the double differential cross section is an ill-posed problem. At best, multiple scattering is treated as a small correction, estimated from sample-specific models. With or without such correction effort, the first and most important measure is using *thin* samples that keep as weak as reasonably possible. Thinner samples require of course longer measuring times, and result in a smaller signal-to-noise ratio. The typical compromise sample scatters about 5 to 10 % of the incident neutrons. For hydrogen-rich materials, this means a sub-mm thickness, which makes powder samples difficult to prepare.

2.2 Instrumental resolution

Every spectrometer has a finite *resolution*. A resolution function is the conditional probability $R(\omega|\omega')$ that a scattering event with energy transfer ω' is registered in the channel ω. Accordingly, a true, 'theoretical' spectrum $S^\mathrm{th}(\omega')$ gives rise to an observed, 'experimental' spectrum

$$S^\mathrm{ex}(\omega) = \int \mathrm{d}\omega'\, R(\omega|\omega') S^\mathrm{th}(\omega'). \tag{3}$$

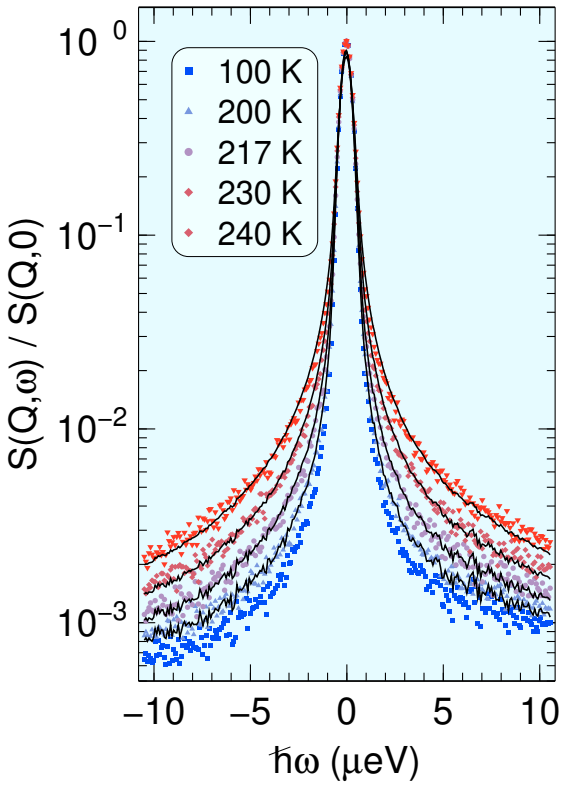

Fig. 3: Spectra of hydration water in deuterated c-phycocyanin protein powder, measured on the backscattering spectrometer SPHERES of JCNS [10]. Solid lines are fit with a Kohlrausch-Williams-Watts function ($\beta = 0.5$, see Eq. (40) below), numerically convolved with the resolution measured at 100 K. As in many other QENS experiments, quasielastic scattering first appears deep in the wings of the resolution function, whereas no broadening can be seen at half maximum.

To make R tractable, one usually assumes $R(\omega|\omega') \simeq R(\omega - \omega')$, which makes of (3) a convolution integral, $S^{\mathrm{ex}} \simeq R \otimes S^{\mathrm{th}}$, and allows for an experimental determination of R by measuring the spectrum of an elastic scatterer.[2]

The resolution functions of time-of-flight and backscattering spectrometers are in a very first approximation Gaussian. Typical scattering functions (Lorentz or Kohlrausch-Williams-Watts functions, see below) are qualitatively different in shape; when scaled for equal maximum and equal width at half maximum, they have much broader wings than a Gaussian. In consequence, the onset of quasielastic scattering is typically detected as additional scattering deep in the wings of the resolution function before any broadening is observed in the width at half maximum (Fig. 3). For this reason, in high-resolution neutron scattering the signal-to-noise ratio is a more important figure of merit than the nominal resolution width.

In principle, resolution effects can be removed from experimental data by Fourier deconvolution:

$$I^{\mathrm{th}}(t) = I^{\mathrm{ex}}(t)/\tilde{R}(t). \tag{4}$$

The number of independent t points is limited by the Nyquist sampling theorem. For most of these t, (4) results in the division of two small, noisy numbers. Therefore one must introduce a cut-off time, restricting I^{th} to a relatively small number of short-time data points. This loss of information is normally not acceptable; instead of deconvoluting experimental data, it is preferable to fit the measured data S^{ex} with a theoretical function S^{th} that has been numerically convolved with the measured resolution R (or a smoothened model thereof). However, explicit

[2] $S^{\mathrm{th}} = \delta$ implies $S^{\mathrm{ex}} = R$. Phonon scattering can be tolerated since it mainly involves energies far outside the resolution peak. Usually, the resolution measurement is done either with vanadium (a perfectly incoherent scatterer so that it can also be used for detector calibration) or with the sample at low temperature (which minimizes variations of sample geometry and environment, and also can be used for intensity normalization).

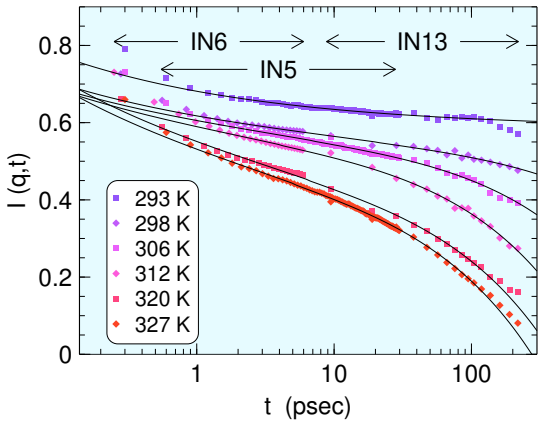

Fig. 4: Intermediate scattering function of the glass-forming liquid ortho-terphenyl, measured on three different spectrometers of the ILL, and combined after Fourier deconvolution [11]. Solid lines are fits with a mode-coupling scaling function.

Fourier deconvolution is attractive for combining spectral measurements from different spectrometers (Fig. 4) or for comparing neutron scattering with molecular dynamics simulations.

3 Interpreting the scattering function

Neutron spectra are usually analysed and presented in form of the scattering function $S(Q,\omega)$, and so for good reasons: $S(Q,\omega)$ depends neither on cross sections nor on the neutron wavelength or any other details of the scattering experiment; it just contains the sample physics the scattering experiment is meant to reveal. Microscopic expressions for $S(Q,\omega)$ or its Fourier transforms $I(Q,t)$ and $G(r,t)$ provide the link from the scattering experiment to microscopic theory or to atomistic simulations or to other information obtained from experiments. This section introduces some basic concepts that are helpful for the interpretation of $S(Q,\omega)$.

3.1 Rebinning from angle to scattering wavenumber

Backscattering or time-of-flight spectrometers have detectors at fixed scattering angles. This facilitates the conversion of raw neutron counts into the double differential cross section, which is a function of 2θ and ω.

For further conversion into the scattering function $S(Q,\omega)$, one needs to replace the dependence on 2θ by one on Q. This is trivial for backscattering where $\hbar|\omega| \ll E_\mathrm{i}$ ensures $Q \simeq 2k_\mathrm{i}\sin\theta$. But in general, Q is a function of 2θ and ω (Fig. 5). Therefore, the experimental data need to be rebinned. Furthermore, for any given Q, only a restricted ω range is accessible. To avoid these difficulties, some experiments are interpreted in terms of $S(2\theta,\omega)\ldots$ and in some papers, spectra are incorrectly labelled $S(Q,\omega)$ although they clearly belong to constant θ.

3.2 The scattering function as an idealization

In first Born approximation, the double differential cross section is given by

$$\frac{\partial^2\sigma}{\partial\Omega\partial\omega} = \frac{k_\mathrm{out}}{k_\mathrm{in}} \int \frac{\mathrm{d}t}{2\pi} \mathrm{e}^{i\omega t} \frac{1}{N} \sum_j^N \sum_l^N \left\langle b_j \mathrm{e}^{i\mathbf{Q}\mathbf{R}_j(0)} b_l \mathrm{e}^{-i\mathbf{Q}\mathbf{R}_l(t)} \right\rangle , \tag{5}$$

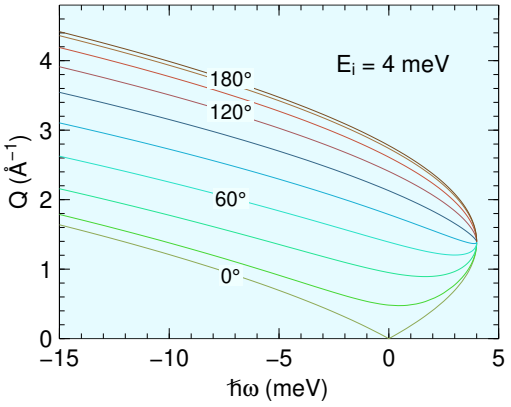

Fig. 5: Dynamic range of a multi-detector time-of-flight spectrometer: At given detector angle 2θ, the scattering wavenumber Q is a function of the energy transfer $\hbar\omega$.

where the scattering lengths b_j, dependent on nuclear spins, and the nuclear positions $\mathbf{R}_j$ are operators, and $\langle \ldots \rangle$ is a quantum-statistical average. Except for nuclear magnetism, spins and positions are uncorrelated so that $\langle b_j b_l \rangle$ can be averaged independently from the positional function $\left\langle \mathrm{e}^{i\mathbf{Q}\mathbf{R}_j(0)} \mathrm{e}^{-i\mathbf{Q}\mathbf{R}_l(t)} \right\rangle$. At this point, to evaluate the averages, one must distinguish whether or not j equals l. This motivates the distinction of *incoherent* and *coherent scattering*.

In textbook-like oversimplification, one would write

$$\frac{\partial^2\sigma}{\partial\Omega\partial\omega} = \frac{k_{\text{out}}}{k_{\text{in}}} \frac{4\pi}{N} \left\{ \sigma_{\text{inc}} S_{\text{inc}}(\mathbf{Q},\omega) + \sigma_{\text{coh}} S_{\text{coh}}(\mathbf{Q},\omega) \right\}, \tag{6}$$

with $\sigma_{\text{inc}} = \langle b^2 \rangle - \langle b \rangle^2$ and $\sigma_{\text{coh}} = \langle b \rangle^2$, and with *scattering functions* S_{inc}, S_{coh} that only depend on position operators. However, most samples contain more than one chemical element, and atoms belonging to different elements move differently. This can be formalized in two different ways: Either one extends (6) by summing over different element-specific scattering functions, or one keeps (6) intact and redefines S_{inc} and S_{coh} as scattering-length weighted functions. The latter choice is prevalent.

Often, one chemical element dominates the scattering cross section so that all other contributions can be neglected in the interpretation of the scattering-length weighted scattering function. This is especially true for samples that contain hydrogen: The incoherent cross section of the isotope ^{1}H is so big that all other elements can be neglected, and the scattering can be entirely attributed to the self-correlation of the hydrogen nuclei. This is the case for most examples in the present chapter.

Two more simplifications facilitate the interpretation of the scattering function: Most QENS experiments address either disordered materials or ordered matter in powder form. In both cases one can take the *powder average*, so that only a scalar Q dependence is left in the scattering function $S(Q,\omega)$. And the *detailed balance* correction

$$\tilde{S}(Q,\omega) := \mathrm{e}^{\hbar\omega/2k_{\mathrm{B}}T} S(Q,\omega) \tag{7}$$

compensates for the different probabilities of up- and downscattering. In the following, we take (7) for granted, and omit the tilde from S.

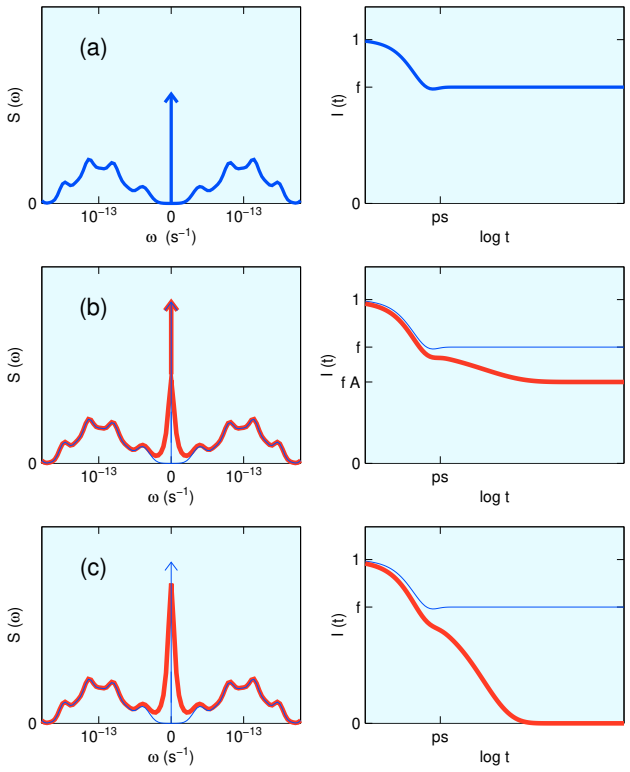

Fig. 6: Hand-drawn $S(Q,\omega)$ and $I(Q,t)$ for some schematic models: (a) An elastic delta line and an inelastic mode distribution. (b) At higher temperatures (red), there is an additional quasileastic component. (c) Here, the central peak of the red spectrum is entirely quasielastic; it has no delta component.

3.3 Frozen, localized, and diffusive dynamics

For brevity, let us specialize to incoherent scattering and drop the subscript 'inc'. For the qualitative physical interpretation of QENS spectra, it is of central importance to switch forth and back between the scattering function

$$S(\mathbf{Q},\omega) = \frac{1}{2\pi}\int \mathrm{d}t\, \mathrm{e}^{-\mathrm{i}\omega t}\, I(\mathbf{Q},t), \tag{8}$$

and its Fourier transform in time, the *intermediate scattering function*

$$I(\mathbf{Q},t) = \frac{1}{N}\sum_j \left\langle \mathrm{e}^{-\mathrm{i}\mathbf{Q}\hat{\mathbf{r}}_j(0)} \mathrm{e}^{i\mathbf{Q}\hat{\mathbf{r}}_j(t)} \right\rangle, \tag{9}$$

which captures *self correlations* of *tagged particles*.

By construction, I has the initial value $I(\mathbf{Q},0) = 1$, from which we obtain the *sum rule*

$$\int_{-\infty}^{+\infty} \mathrm{d}\omega\, S(Q,\omega) = 1. \tag{10}$$

No such rule holds for $S(2\theta,\omega)$ or for $\partial^2\sigma/\partial\Omega/\partial\omega$. Also note that experiments only cover restricted ω ranges (Fig. 5). Therefore, integration of experimental scattering functions will usually yield less than 1, except in absence inelastic scattering. This is the rationale for the *normalization* of experimental spectra to a low-temperature measurement.

Fig. 6 shows Fourier transform pairs $S(Q,\omega)$, $I(Q,t)$ for three idealized situations. In (a), there is a phonon spectrum but no quasielastic scattering. Accordingly, the central peak at $\omega = 0$ is a

delta line. The Fourier transform of a delta function is a constant. Therefore $I(Q,t)$ decays from its initial value 1 towards a long-time limit $f_Q > 0$. This f_Q is just the amplitude of the delta component of $S(Q,\omega)$, and is called the *Debye-Waller factor*, or, specifically for incoherent scattering, the *Lamb-Mössbauer factor*.

In (b), there is *some* quasielastic scattering, but on top of it there still an elastic delta line of amplitude $f_Q A_Q$. In the Fourier transform, scattering at small $|\omega|$ corresponds to relaxation on long time scales, therefore $I(Q,t)$ decays in two steps that can be more or less pronounced. Since correlations remain finite, the second step is ascribed to *localized motion*. The factor A_Q is called the *elastic incoherent structure factor* (EISF).

In (c), the entire central peak is quasielastic; there is no delta component. Accordingly, $I(Q,t)$ decays to 0. This implies long-ranged diffusive motion.

To summarize these three cases, we write the scattering function as

$$S(Q,\omega) = f_Q S_{\text{slow}}(Q,\omega) + (1-f_Q) S_{\text{fast}}(Q,\omega). \tag{11}$$

The fast component is typically the phonon spectrum; it lies almost entirely outside the dynamic range of a backscattering spectrometer. The slow component

$$S_{\text{slow}}(Q,\omega) = A_Q \delta(\omega) + S_{\text{QENS}}(Q,\omega) \tag{12}$$

consists of the elastic delta line, with amplitude given by the EISF, and of a quasielastic spectrum. In case (a), $A_Q = 1$ and $S_{\text{QENS}} = 0$; in case (c), $A_Q = 0$. So only in case (b) all three components are present.

4 Sample physics models

For certain types of samples, there exist idealized models that can be solved analytically, yielding closed expressions for the scattering function. These models include harmonic vibrations, intramolecular rotation, diffusion, and structural relaxation, briefly described in the following subsections. Even where these models do not apply literally they provide an indispensable reference for discussing crossover scenarios, correction terms, or refined models.

4.1 Harmonic vibrations and the mean squared displacement

For harmonic vibrations, S_{fast} and f_Q can be derived in closed form. While the phonon spectrum is out of scope here, the result for f_Q is of the outmost importance for the analysis of QENS data. Vibrations are described in terms of displacements $\mathbf{u}_j(t)$ from equilibrium positions $\mathbf{R}_j$,

$$\mathbf{r}_j(t) = \mathbf{R}_j + \mathbf{u}_j(t). \tag{13}$$

If there are only harmonic forces, then the Bloch theorem [13] reduces (9) to

$$I(\mathbf{Q},t) = \frac{1}{N} \sum_j \mathrm{e}^{-2W_j(\mathbf{Q},\mathbf{0})} \mathrm{e}^{2W_j(\mathbf{Q},t)} \tag{14}$$

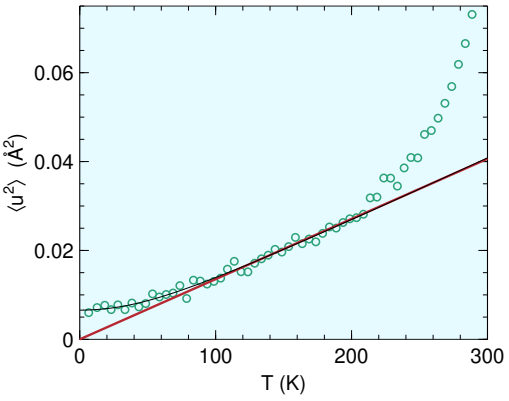

Fig. 7: Temperature dependence of the mean squared displacement in glycerol $C_3H_5(OD)_3$, obtained from elastic thermal neutron backscattering [12]. The black line is a fit with the Debye model. The red line is the linear high-temperature asymptote of that model. Deviations from the fit above the glass transition ($T_g = 185$ K) are due to quasielastic broadening.

with

$$2W_j(\mathbf{Q},t) \coloneqq \langle\, (\mathbf{Q}\mathbf{u}_j(0))(\mathbf{Q}\mathbf{u}_j(t)) \,\rangle\,. \tag{15}$$

In isotropic systems, an orientational average gives

$$2W_j(Q,t) = \frac{Q^2}{3} \langle\, \mathbf{u}_j(0)\mathbf{u}_j(t) \,\rangle\,. \tag{16}$$

Each particle partakes in a huge number of oscillatory modes, which quickly run out of phase. Therefore, within little more than one typical phonon period, $2W_j(\mathbf{Q},t)$ approaches 0.

Assuming that there is just one kind of scatterers,

$$f_Q \equiv I(\mathbf{Q}, t\to\infty) = \mathrm{e}^{-Q^2\langle \mathbf{u}^2\rangle/3}. \tag{17}$$

So the Lamb-Mössbauer factor reveals the *mean squared displacement* (MSD).[3] Experimentally, one may obtain the MSD from the slope of $-\ln f_Q$ versus Q^2. However, one must expect serious distortions from multiple scattering [9, 15].

Harmonic theory provides a closed expression for the MSD in terms of the *vibrational density of states* $g(\omega)$,

$$\langle u_x^2\rangle = \frac{\hbar}{6m}\int \mathrm{d}\omega\, \frac{g(\omega)}{\omega} \coth\frac{\hbar\omega}{2k_\mathrm{B}T}. \tag{18}$$

Specially for the *Debye model*, one finds that the MSD as function of temperature crosses over from a constant plateau, due to zero-point oscillations, to linear growth. At even higher temperatures, deviations from the linearity $\langle x^2\rangle \propto T$ may then reveal anharmonicity or quasielastic broadening (Fig. 7).

4.2 Two-site jumps

Probably the simplest model of anharmonic localized motion consists of a proton that jumps between two positions $\mathbf{r}_1$ and $\mathbf{r}_2$. In practice, this motion may combine with confined diffusion so that one should rather talk of jumps between two cages. Fig. 8 shows that this actually

[3] There is widespread confusion in notation and about factors 2 and 3 [14]: If one refers to just one Cartesian component $x \equiv u_x$ of the displacement, then one may write $\langle x^2\rangle = \langle \mathbf{u}^2\rangle/3$. And the relative displacement of two independent scatterers is $\langle \mathbf{r}^2\rangle = 2\langle \mathbf{u}^2\rangle$.

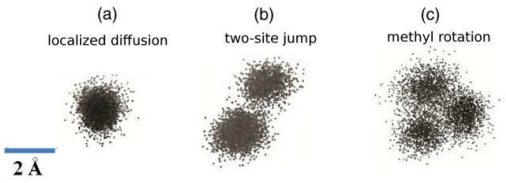

Fig. 8: Scatter plots of time-sampled position of three different hydrogen atoms in Green Fluorescent Protein, from a molecular dynamics simulation. Reproduced with kind permission from [16].

happens for some hydrogen atoms in a protein, while other H atoms are confined to *one* cage, or partake in methyl group rotation, to be discussed in the next subsection.

The probability $p(\mathbf{r}, t)$ of finding the proton at time t at site $\mathbf{r}$ obeys the rate equation

$$\frac{\mathrm{d}}{\mathrm{d}t}\begin{pmatrix} p(\mathbf{r}_1,t) \\ p(\mathbf{r}_2,t) \end{pmatrix} = -\begin{pmatrix} \lambda_1 & -\lambda_2 \\ -\lambda_1 & \lambda_2 \end{pmatrix}\begin{pmatrix} p(\mathbf{r}_1,t) \\ p(\mathbf{r}_2,t) \end{pmatrix} \tag{19}$$

with transition rates λ_n. The matrix has the eigenvalues 0 and $\Gamma := \lambda_1 + \lambda_2$. The rate equation is solved by $p(\mathbf{r}_n, t) = a_n + b_n \exp(-\Gamma t)$. In the limit $t \to \infty$, the occupation ratio must be $p_1/p_2 = \lambda_2/\lambda_1$ to satisfy $\mathrm{d}p/\mathrm{d}t = 0$. Combined with the normalization condition $\sum_n p(\mathbf{r}_n, t) = 1$, we find

$$a_1 = p(\mathbf{r}_1, \infty) = \lambda_2/\Gamma, \quad a_2 = p(\mathbf{r}_2, \infty) = \lambda_1/\Gamma. \tag{20}$$

Making the probabilities conditional upon the initial condition $p(\mathbf{r}_1, 0) = 1$, we compute

$$\begin{aligned} p(\mathbf{r}_1, t|\mathbf{r}_1, 0) &= a_1 + a_2 \exp(-\Gamma t), \\ p(\mathbf{r}_2, t|\mathbf{r}_1, 0) &= a_2 \left(1 - \exp(-\Gamma t)\right), \end{aligned} \tag{21}$$

and similarly for $p(\mathbf{r}_2, 0) = 1$. Using the equilibrium occupation probabilities (20) we obtain the intermediate self correlation function

$$\begin{aligned} I(\mathbf{Q}, t) &= \langle \mathrm{e}^{\mathrm{i}\mathbf{Q}\mathbf{r}(t)} \mathrm{e}^{-\mathrm{i}\mathbf{Q}\mathbf{r}(0)} \rangle \\ &= p(\mathbf{r}_1, \infty)\left[p(\mathbf{r}_1, t|\mathbf{r}_1, 0) + p(\mathbf{r}_2, t|\mathbf{r}_1, 0)\mathrm{e}^{\mathrm{i}\mathbf{Q}\mathbf{d}}\right] + \\ &\quad p(\mathbf{r}_2, \infty)\left[p(\mathbf{r}_2, t|\mathbf{r}_1, 0) + p(\mathbf{r}_1, t|\mathbf{r}_1, 0)\mathrm{e}^{-\mathrm{i}\mathbf{Q}\mathbf{d}}\right] \end{aligned} \tag{22}$$

with the jump vector $\mathbf{d} := \mathbf{r}_2 - \mathbf{r}_1$. Regrouping terms, abbreviating

$$\begin{aligned} A_0(\mathbf{Q}) &:= a_1^2 + a_2^2 + 2a_1 a_2 \cos \mathbf{Q}\mathbf{d}, \\ A_1(\mathbf{Q}) &:= 2a_1 a_2 (1 - \cos \mathbf{Q}\mathbf{d}), \end{aligned} \tag{23}$$

and evaluating the Fourier transform of $\exp(-\Gamma t)$, we get the incoherent scattering function

$$S(\mathbf{Q}, \omega) = A_0(\mathbf{Q})\delta(\omega) + A_1(\mathbf{Q})\mathcal{L}(\omega; \Gamma), \tag{24}$$

which consists of an elastic line and a quasielastic component. The latter is *Lorentzian*,

$$\mathcal{L}(\omega; \Gamma) := \frac{1}{\pi}\frac{\Gamma}{\Gamma^2 + \omega^2}. \tag{25}$$

As discussed above, the presence of an elastic line is characteristic for *localized motion*: Since the jumping proton is confined to a finite region in space, its self correlation function never decays to zero.

For powder samples, we average over the orientations of $\mathbf{d}$,

$$\overline{\cos \mathbf{Qd}} = \frac{1}{4\pi} \int_0^\pi \mathrm{d}\vartheta \, 2\pi \sin\vartheta \, \cos(Qd\cos\vartheta) = \frac{\sin Qd}{Qd} = j_0(Qd) \tag{26}$$

with the spherical Bessel function j_0. In the simplest case, for jumps between two equivalent positions, we have $\lambda_1 = \lambda_2$ and $a_1 = a_2 = 1/2$, so that

$$\begin{aligned} A_0(Q) &= (1 + j_0(Qd))/2, \\ A_1(Q) &= (1 - j_0(Qd))/2. \end{aligned} \tag{27}$$

4.3 Rotational jump diffusion

Rotation of molecules or molecular sidegroups is a strong and often dominant source of quasi-elastic scattering. As the simplest and most important example, we consider the rotation of a methyl group. In polymers and proteins, this degree of freedom has important effects upon structure and mechanical properties.

We consider the group R–CH_3 as stiff (CH bond length $d = 1.097 \pm 0.004$ Å, HCH angle $\theta = 106.5 \pm 1.5°$). The only degree of freedom is the rotation around the R–C bond. The moment of inertia is

$$I = \sum m d_\perp^2 = 2md^2(1 - \cos\theta). \tag{28}$$

The rotational motion can be described by a wave function ψ that depends on one single coordinate, the rotation angle ϕ. The Schrödinger equation is

$$\left\{ B\frac{\partial^2}{\partial\phi^2} - V(\phi) + E \right\} \psi(\phi) = 0 \tag{29}$$

with the *rotational constant*

$$B \coloneqq \frac{\hbar^2}{2I} = 670 \ \mu\mathrm{eV}. \tag{30}$$

For free rotation ($V = 0$), solutions that possess the requested periodicity are sine and cosine functions of argument $J\phi$, with integer J. Accordingly, the energy levels are $E = BJ^2$.

In condensed matter, however, the potential V caused by the local environment cannot be neglected. Due to the symmetry of the CH_3 group, the Fourier expansion of $V(\phi)$ contains only sine and cosine functions with argument $3m\phi$, with integer m. In most applications, it is sufficient to retain only one term,

$$V(\phi) \doteq V_3 \cos(3\phi). \tag{31}$$

The strength of the potential can then be expressed by the dimensionless number V_3/B. In the following we specialize to the case of a *strong potential*, $V_3/B \gg 10$, which is by far the most frequent one.

In a strong potential of form (31), the CH_3 group has three preferential orientations (Fig. 8c), separated by potential walls. The motion of the CH_3 group consists mainly of small excursions from the preferred orientations, called *libration*. Quantum-mechanically, they are zero-point oscillations in an approximately harmonic potential. Occasionally though, there are *thermally*

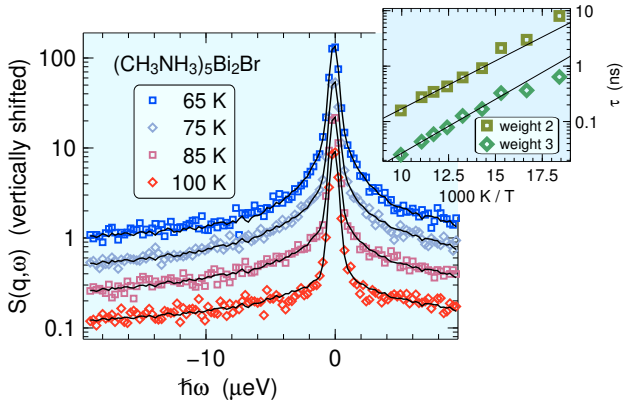

Fig. 9: Backscattering spectra of $(CH_3NH_3)_5Bi_2Br$, measured on SPHERES [17]. The five methylammonium cations fall into two different categories: at room temperature, two of them are ordered, three are disordered [18]. Therefore, we fitted the spectra with two Lorentzians with an amplitude ratio of 2:3. The resulting relaxation times have an Arrhenius temperature dependence, shown in the inset.

activated jumps between the three cages. Modelling this *jump diffusion* requires only a little extension of the two-site jump model introduced above. The transition matrix in the rate equation takes the form

$$\begin{pmatrix} 2\lambda & -\lambda & -\lambda \\ -\lambda & 2\lambda & -\lambda \\ -\lambda & -\lambda & 2\lambda \end{pmatrix}, \tag{32}$$

which has the eigenvalues 0, 3λ, 3λ. Thanks to the degeneracy of the nonzero eigenvalue, the scattering law retains the simple form (24), with $\Gamma = 3\lambda$, and with amplitudes

$$\begin{aligned} A_0(Q) &= (1 + 2j_0(Qr\sqrt{3}))/3, \\ A_1(Q) &= (2 - 2j_0(Qd\sqrt{3}))/3, \end{aligned} \tag{33}$$

where r is the radius of the circle on which the rest positions are located. This model has proven successful in a huge number of experiments; Fig. 9 shows an arbitrarily chosen recent example.

If the rotational potential has a C_2 symmetry, then there are six equivalent equilibrium positions, connected by 60° jumps, so that the transition matrix is of rank 6. After some computation it is found to have three different non-zero eigenvalues Γ_μ. In such a situation, the inelastic part of scattering law no longer factorises into a Q dependent and a ω dependent function. Instead, one has a sum of Lorentzians of different widths:

$$S(\mathbf{Q}, \omega) = A_0(\mathbf{Q})\delta(\omega) + \sum_\mu A_\mu(\mathbf{Q})\mathcal{L}(\omega; \Gamma_\mu). \tag{34}$$

This equation holds quite generally for systems described by a rate equation of the form (19) with an arbitrary, symmetric transition matrix. In particular, it holds for rotational jump diffusion of molecules that have more than one axis of rotation [4].

4.4 Rotational tunneling

At low temperatures, almost exclusively the vibrational ground state is occupied. Yet reorientational motion beyond librations is possible by means of quantum mechanical tunneling: The wave functions of the three localised *pocket states* ψ_m ($m = 1, 2, 3$) have nonzero overlap. Therefore, the eigenstates are a linear combination of pocket states.[4] Periodicity and threefold

[4] This is an extremely simplified outline of the theory. In a serious treatment, to get all symmetry requirements right, one must also take into account the nuclear spins of the H atoms [3].

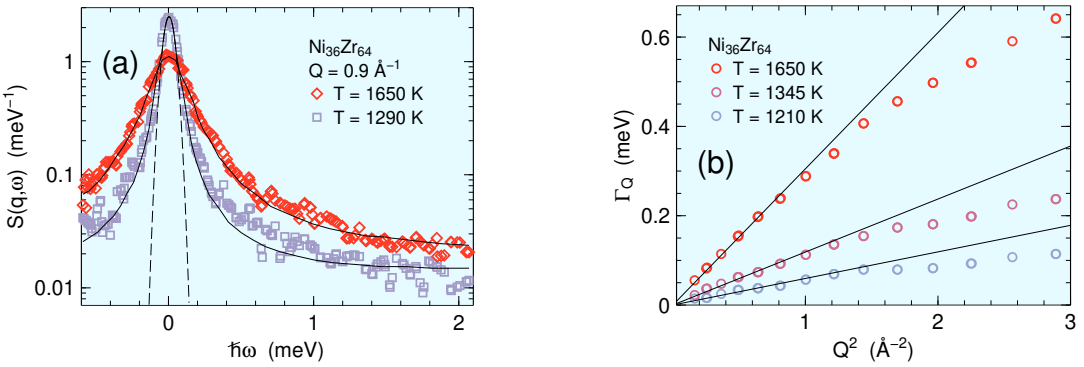

Fig. 10: Atomic dynamics of liquid Zr-Ni, investigated with the time-of-flight spectrometer TOFTOF [19]. (a) Selected spectra with Lorentzian fits (39). The dashed Gaussian with a FWHM of 95 μeV approximates the instrumental resolution. (b) Linewidths Γ_Q, from Lorentzian fits to the spectra. For small Q, scattering is dominated by incoherent contributions from Ni so that the initial slope of Γ_Q vs. Q^2 yields the self-diffusion coefficient of Ni.

symmetry allow three such combinations: a plain additive one

$$\psi_1 + \psi_2 + \psi_3, \tag{35}$$

and two superpositions with phase rotations

$$\psi_1 + \mathrm{e}^{\pm i2\pi/3}\psi_2 + \mathrm{e}^{\pm i4\pi/3}\psi_3. \tag{36}$$

In the language of group theory, state (35) has symmetry A, the degenerate states (36) are labelled E^a, E^b. It is found that A is the ground state. The *tunneling splitting* $\hbar\Omega_\mathrm{t}$ between the states A and E is determined by the overlap integral $\langle\psi_m|V|\psi_n\rangle$ ($m \neq n$), which depends exponentially on the height of the potential wall. Experiments that detect tunneling transitions provide therefore a very sensitive probe of the rotational potential; conversely, if the potential is not accurately known, it is almost impossible to predict whether a tunneling transition will show up in a given experimental energy range.

In neutron scattering, a tunneling transition appears as a pair of inelastic peaks at $\pm\hbar\Omega_\mathrm{t}$. The spectral shape of these peaks is well described by Lorentzians $\mathcal{L}(\omega\pm\Omega_\mathrm{t};\Gamma)$. With rising temperatures, the occupancy of excited vibrational levels increase. This facilitates transitions between A and E sublevels and results in a decrease of $\hbar\Omega_\mathrm{t}$ and an increase of the line width Γ. Upon further temperature increase, thermal motion of neighbouring molecules causes so strong potential fluctuations that the picture of quantum tunneling is no longer applicable. Instead, the motion between different pocket states must be described as thermally activated jump diffusion, as exposed in the previous subsection. An experimental example has already been given in Fig. 1.

4.5 Diffusion

The simplest model for *self-diffusion* is Brownian motion. It can be described as a memory-less *random walk*. Particle trajectories $\mathbf{r}(t)$ are subject to the *Langevin equation*. Equivalently, the *diffusion equation* is applied to the Van Hove self-correlation function, resulting in the solution

$$G_\mathrm{s}(\mathbf{r},t) = (4\pi Dt)^{-3/2}\mathrm{e}^{-r^2/4Dt}. \tag{37}$$

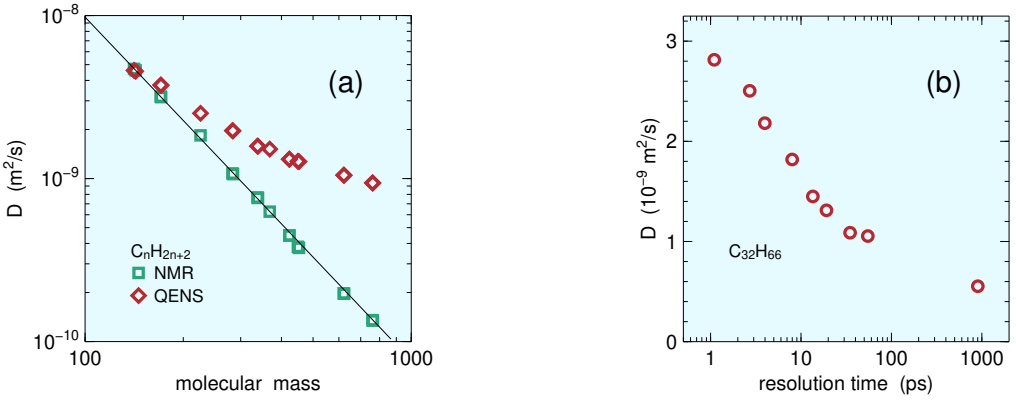

Fig. 11: Hydrogen dynamics in n-alkanes. (a) Diffusion coefficient D, determined by pulsed-field gradient NMR and by neutron scattering. The data agree only for the shortest molecule ($n = 8$). In longer chains, QENS deviates from NMR because it measures not only center-of-mass molecular translation, but also rotation and intramolecular motion [20]. (b) In an exemplary series of TOFTOF measurements with different instrumental resolutions naive fits result in a dependence of the apparent diffusion coefficients on the *resolution time* [21].

By Fourier transform, we find the intermediate scattering function

$$I(Q,t) = \exp(-DQ^2t) \tag{38}$$

and the scattering function

$$S(Q,\omega) = \mathcal{L}(\omega; DQ^2). \tag{39}$$

On a time-of-flight spectrometer, with experimental scales of the order $Q \sim \text{Å}^{-1}$ and $\hbar\omega \sim 0.1 \ldots 10$ meV, one can resolve diffusion coefficients D of the order $10^{-10} \ldots 10^{-8}$ m^2/s.

As anticipated in Sect. 3.3 and Fig. 6, there is no elastic scattering component, in contrast to the localized jump models of Sects. 4.2–4.4. In practice, however, there may be some elastic scattering from the sample container.[5] And in an important class of applications, one investigates diffusion in a solid matrix, e. g. hydrogen diffusion in metals [5]. Therefore, absence of elastic scattering is not a reliable indicator of long-ranged diffusion. The key indicator is rather the pronounced Q dependence of the Lorentzian width $\Gamma = DQ^2$, in contrast to the Q-independent width of the jump models. Conversely, (39) has a fixed amplitude 1, whereas the Lorentzians of the jump models oscillate with Q.

The straightforward determination of D from Lorentzian fits (39) works best in simple atomic systems. Recent examples are provided by metallic melts, which can be studied under very clean experimental conditions using electromagnetic levitation (Fig. 10). Results improve significantly upon macroscopic laboratory measurements that suffer from convective contributions.

In molecular liquids the applicability of (39) is not ascertained a priori because the atomic motion seen by neutron scattering is a superposition of translations, rotations, vibrations and rearrangements. This has been demonstrated very clearly in a systematic study of alkanes C_nH_{2n+2} (Fig.11) [20, 21].

[5] It is debatable whether container scattering should be subtracted from the raw data, or taken into account as part of the fit model. Either way of correcting is only approximative because of sample-container multiple scattering.

4.6 Structural relaxation

Atoms or molecules that constitute a *liquid* also undergo long-range diffusion. On short time and length scales, however, their trajectories are *not* memory-less random walks. Particles rather rattle in transient cages, occasionally probe a step out of the cage, and more often than not do the next step in the backward direction. This delays the decay of correlations, and is well described by Kohlrausch's *stretched exponential function*

$$\exp(-(t/\tau)^{\beta}) \tag{40}$$

that is also known from other experimental probes of *structural relaxation* [22]. Typical values of β are between 0.4 and 0.8.

To use (40) in spectral fits, its Fourier transform, the *Kohlrausch-Williams-Watts function*, must be computed numerically [23]. Fig. 3 shows an application to the motion of supercooled hydration water in a protein powder.

Empirical fit functions like (40) do not capture the short-time dynamics of rattling particles. For this, one needs a microscopic theory, as proposed by the *mode-coupling theory* of structural relaxation [24, 25]. This theory starts from a closed equation of motion for density correlations, and leads to scaling functions like those used in the fits of Fig. 4.

I thank Winfried Petry for introducing me to neutron backscattering, Wolfgang Doster for discussions of data interpretation, Tapan Chatterji, Grazyna Bator, Michael Prager, Tobias Unruh, and many more colleagues, for joint experiments, Marie-Sousai Appavou, Barbara Daegener, Daria Noferini, Reiner Zorn for corrections on the manuscript.

References

[1] G. Bator *et al.*, Chem. Phys. **410**, 55 (2013).

[2] T. Unruh and J. Wuttke, *MLZ Experimental Report 2512* (2009).

[3] W. Press, *Single-particle rotation in molecular crystals* (Springer tracts in modern physics 92), Springer: Berlin (1981).

[4] M. Bée, *Quasielastic Neutron Scattering*, Adam Hilger: Bristol (1988).

[5] R. Hempelmann, *Quasielastic Neutron Scattering and Solid State Diffusion*, Clarendon Press: Oxford (2000).

[6] M. T. F. Telling and V. Garcia Sakai, *A Practical Guide to Quasi-Elastic Neutron Scattering*, Royal Society of Chemistry (2019).

[7] G. H. Vineyard, Phys. Rev. **96**, 93 (1954).

[8] V. P. Sears, Adv. Phys. **24**, 2 (1975).

[9] J. Wuttke, Phys. Rev. E **62**, 6531 (2000).

[10] W. Doster *et al.*, Phys. Rev. Lett. **104**, 098101 (2010).

[11] J. Wuttke *et al.*, Z. Phys. B **91**, 357 (1993).

[12] J. Wuttke, W. Petry, G. Coddens and F. Fujara, Phys. Rev. E **52**, 4026 (1995).

[13] N. W. Mermin, J. Math. Phys. **7**, 1038 (1966).

[14] W. Doster, Eur. Biophys. J. **37**, 591 (2008).

[15] R. Zorn, Nucl. Inst. Meth. A **572**, 874 (2007).

[16] L. Hong *et al.*, Phys. Rev. Lett. **110**, 028104 (2013).

[17] A. Piecha, J. Wuttke, R. Jakubas and G. Bator, *MLZ experimental report 3961* (2010).

[18] J. Matuszewski, R. Jakubas, L. Sobczyk and T. Głowiak, Acta Cryst. C **46**, 1385 (1990).

[19] D. Holland-Moritz *et al.*, Phys. Rev. B **79**, 064204 (2009).

[20] C. Smuda, S. Busch, G. Gemmecker and T. Unruh, J. Chem. Phys. **129**, 014513 (2008).

[21] T. Unruh *et al.*, J. Chem. Phys. **129**, 121106 (2008).

[22] R. Böhmer, K. L. Ngai, C. A. Angell and D. J. Plazek, J. Chem. Phys. **99**, 4201 (1993).

[23] J. Wuttke, Algorithms **5**, 604 (2012).

[24] T. Voigtmann, in *Soft Matter. From Synthetic to Biological Materials*, edited by J. K. G. Dhont *et al.* (Lecture Notes of the 39th Spring School), Forschungszentrum Jülich: Jülich (2008).

[25] W. Götze, *Complex Dynamics of Glass-Forming Liquids. A Mode-Coupling Theory*, Oxford University Press: Oxford (2009).